Extending the DAMA annual-modulation region by inclusion of the uncertainties in astrophysical velocities

P. Belli,[1,*] R. Bernabei,[1,†] A. Bottino,[2,‡] F. Donato[3,§] N. Fornengo,[4,‖] D. Prosperi,[5,¶] and S. Scopel[6,**]
[1]*Dipartimento di Fisica, Università di Roma ''Tor Vergata,'' and INFN, Sez. di Roma 2, I–00133 Roma, Italy*
[2]*Dipartimento di Fisica Teorica, Università di Torino, and INFN, Sez. di Torino, Via P. Giuria 1, I–10125 Torino, Italy*
[3]*Laboratoire de Physique Théorique LAPTH, B.P. 110, F–74941, Annecy–le–Vieux Cedex, France and INFN, Sez. di Torino, Via P. Giuria 1, I–10125 Torino, Italy*
[4]*Instituto de Física Corpuscular—C.S.I.C.—Departamento de Física Teòrica, Universitat de València, E-46100 Burjassot, València, Spain*
[5]*Dipartimento di Fisica, Università di Roma ''La Sapienza,'' and INFN, Sez. di Roma, I–00185, Roma, Italy*
[6]*Instituto de Física Nuclear y Altas Energías, Facultad de Ciencias, Universidad de Zaragoza, Plaza de San Francisco s/n, E–50009 Zaragoza, Spain*
(Received 26 March 1999; published 23 December 1999)

The original annual-modulation region, singled out by the DAMA-NaI experiment for direct detection of WIMPs, is extended by taking into account the uncertainties in the galactic astrophysical velocities. Also the effect due to a possible bulk rotation for the dark matter halo is considered. We find that the range for the WIMP mass becomes 30 GeV$\lesssim m_\chi \lesssim$130 GeV at 1σ C.L. with a further extension in the upper bound, when a possible bulk rotation of the dark matter halo is taken into account. We show that the DAMA results, when interpreted in the framework of the minimal supersymmetric extension of the standard model, are consistent with a relic neutralino as a dominant component of cold dark matter (on the average in our universe and in our galactic halo). The discovery potential for the relevant supersymmetric configurations at present generation accelerators is also discussed.

PACS number(s): 95.35.+d, 11.30.Pb, 12.60.Jv

I. INTRODUCTION

The DAMA-NaI Collaboration has recently reported indication of an annual-modulation effect in a direct search experiment for weakly interacting massive particles (WIMPs) [1–3]. In Ref. [3] it has been shown that a statistical (maximum-likelihood) analysis of the data concerning a total exposure of 19,511 kg×day provides, at a 2σ C.L., a well delimited region in the plane $\rho_\chi \sigma_{\rm scalar}^{\rm (nucleon)} - m_\chi$, where m_χ is the WIMP mass, ρ_χ is its local (solar neighborhood) density, and $\sigma_{\rm scalar}^{\rm (nucleon)}$ is the WIMP-nucleon scalar elastic cross section. Obviously, the location of the annual-modulation region depends on the functional form adopted for the speed distribution of the dark matter particles, and on the values assigned to the galactic astrophysical velocities. In Refs. [1–3] a standard Maxwellian distribution was taken for the WIMP speed distribution with a root mean square velocity $v_{\rm rms} = 270$ km s^{-1} and a WIMP escape velocity in the halo $v_{\rm esc} = 650$ km s^{-1}.

The DAMA-NaI results on annual modulation were analyzed in Refs. [4–8] in terms of relic neutralinos. It was proved that the DAMA-NaI data are compatible with a neutralino as a major component of dark matter in the universe. In Refs. [4–8] it was also shown that a significant number of the relevant supersymmetric configurations are compatible with supergravity schemes [9] and are explorable at accelerators and/or by indirect searches for relic particles (upgoing muons at neutrino telescopes and antiprotons in space).

In the present paper we discuss (i) the extension of the DAMA-NaI annual-modulation region in the plane $\rho_\chi \sigma_{\rm scalar}^{\rm (nucleon)} - m_\chi$, when the uncertainties of the galactic astrophysical velocities are taken into account and (ii) the ensuing consequences of this extension in terms of properties for relic neutralinos and for the related supersymmetric configurations [10].

II. EXTENDED ANNUAL-MODULATION REGION

The differential rate for WIMP direct detection is given by

$$\frac{dR}{dE_R} = N_T \frac{\rho_\chi}{m_\chi} \int_{v_{\rm min}}^{v_{\rm max}} d\vec{v} f(\vec{v}) v \frac{d\sigma}{dE_R}(v, E_R), \qquad (1)$$

where N_T is the number of the target nuclei per unit of mass, $\vec{v}$ and $f(\vec{v})$ denote the WIMP velocity and velocity distribution function in the Earth frame ($v = |\vec{v}|$), and $d\sigma/dE_R$ is the WIMP-nucleus differential cross section. The nuclear recoil energy is given by $E_R = m_{\rm red}^2 v^2 (1 - \cos\theta^*)/m_N$, where θ^* is the scattering angle in the WIMP-nucleus center-of-mass frame, m_N is the nuclear mass and $m_{\rm red}$ is the WIMP-nucleus reduced mass. The velocity $v_{\rm min}$ is defined as $v_{\rm min}$

*Email address: belli@roma2.infn.it
†Email address: bernabei@roma2.infn.it
‡Email address: bottino@to.infn.it
§Email address: donato@lapp.in2p3.fr
‖Email address: prosperi@roma1.infn.it
¶Email address: fornengo@flamenco.ific.uv.es
**Email address: scopel@posta.unizar.es

$=(m_N E_R/2m_{\rm red}^2)^{1/2}$ and $v_{\rm max}$ is the maximal (escape) WIMP velocity in the Earth reference frame. Equation (1) refers to a monoatomic detector; the generalization to our case of NaI is straightforward.

In general, the differential WIMP-nucleus cross section is composed of a coherent part and a spin-dependent one. Actually, over almost the entire supersymmetric parameter space, the coherent part is largely dominant [11–14]. Therefore, we may write

$$\frac{d\sigma}{dE_R}=\frac{\sigma_0}{E_R^{\rm max}}F^2(q), \tag{2}$$

where σ_0 is the pointlike scalar WIMP-nucleus cross section, $E_R^{\rm max}$ is the maximum value of E_R, and $F(q)$ denotes the nuclear form factor, expressed as a function of the momentum transfer $q^2\equiv|\vec{q}|^2=2m_N E_R$. σ_0 may be conveniently rewritten in terms of the scalar WIMP-nucleon cross section $\sigma_{\rm scalar}^{\rm (nucleon)}$:

$$\sigma_0=\left(\frac{1+m_\chi/m_p}{1+m_\chi/m_N}\right)^2 A^2\sigma_{\rm scalar}^{\rm (nucleon)}, \tag{3}$$

where m_p is the proton mass and A is the mass number of the nucleus.

For the nuclear form factor in Eq. (2) we use the Helm parametrization of the scalar form factor [15,16]

$$F(q)=3\frac{j_1(qr_0)}{qr_0}\exp\left(-\frac{1}{2}s^2q^2\right), \tag{4}$$

where $s\simeq 1$ fm is the thickness parameter for the nucleus surface, $r_0=(r^2-5s^2)^{1/2}$, $r=1.2\,A^{1/3}$ fm, and $j_1(qr_0)$ is the spherical Bessel function of index 1.

Once a functional form for $f(v)$ is chosen and specific values are assigned to the relevant astrophysical velocities, the quantity $\rho_\chi\sigma_{\rm scalar}^{\rm (nucleon)}$ may be extracted from measurements of the differential rate dR/dE_R as a function of m_χ.

Here, for $f(v)$ we take the standard Maxwell–Boltzmann distribution (as in an isothermal spherical model for the halo) with a finite escape velocity, i.e., in the galactic rest frame we write

$$f_{\rm gal}(v^{\rm gal})=N\left(\frac{3}{2\pi v_{\rm rms}^2}\right)^{3/2}\exp\left(-\frac{3(v^{\rm gal})^2}{2v_{\rm rms}^2}\right), \tag{5}$$

where the normalization factor is

$$N=\left[\mathrm{erf}(z)-\frac{2}{\sqrt{\pi}}z\exp(-z^2)\right]^{-1}, \tag{6}$$

with $z^2=3v_{\rm esc}^2/(2v_{\rm rms}^2)$. In the isothermal spherical model, $v_{\rm rms}$ is related to the asymptotic value v_∞ of the rotational velocities by the relation $v_{\rm rms}=\sqrt{\frac{3}{2}}v_\infty$. The measured rotational velocity remains almost flat (to roughly 15%) between 4 and 18 kpc; here, we identify v_∞ with the rotational velocity of the local system at the position of the Solar System $v(r_\odot)\equiv v_0$, whose physical range will be shortly discussed. The assumption employed here that $v_\infty=v_0$ is the one commonly used in the literature (see, for instance, Refs. [12,17,18]), although one should be aware that the determination of v_∞ may be affected by some uncertainties (for example, the disk might provide a non-negligible contribution to the rotation speed at distances larger than the solar radius [12]).

To make use of Eqs. (1), (5) has to be transformed to the rest frame of the Earth, which moves through the Galaxy with a velocity

$$v_\oplus=v_\odot+v_{\rm orb}\cos\gamma\cos[\omega(t-t_0)], \tag{7}$$

in the azimuthal direction. $v_\odot$ is given by

$$v_\odot=v_0+12\ \ {\rm km\,s^{-1}}. \tag{8}$$

In these expressions the speed of 12 $\mathrm{km\,s^{-1}}$ stands for the motion of the Solar System with respect to the local system, $v_{\rm orb}=30$ $\mathrm{km\,s^{-1}}$ denotes the Earth orbital speed around the Sun, the angle $\gamma\simeq 60°$ is the inclination of the Earth orbital plane with respect to the galactic plane and $\omega=2\pi/365$ days, $t_0=$ June 2nd [17,19]. Clearly, the velocity $\vec{v}$ of the WIMPs, as seen in the Earth's frame, is related to their velocity in the Galactic frame $\vec{v}^{\rm gal}$ by the following set of transformation equations: $v_\phi=v_\phi^{\rm gal}-v_\oplus$ in the azimuthal direction and $v_\perp=v_\perp^{\rm gal}$ and $v_R=v_R^{\rm gal}$ in the vertical ($\perp$) and in the radial (R) direction with respect to the galactic plane. The velocity distribution function of Eq. (5) is therefore transfomed as $f_{\rm gal}(v^{\rm gal})d^3v^{\rm gal}=f(v)d^3v$.

In Refs. [1–3] the DAMA-NaI annual-modulation region was extracted from the experimental data, by using a maximum likelihood method and by taking for the velocities v_0 and $v_{\rm esc}$ the following values: $v_0=220$ $\mathrm{km\,s^{-1}}$ and $v_{\rm esc}=650$ $\mathrm{km\,s^{-1}}$ (the relevant region is one of the domains displayed in Fig. 1). The ensuing implications for relic neutralinos, derived in Refs. [4–8], refer to the same set of astrophysical velocities.

In the present paper we extend the analysis of the annual-modulation region, by considering the physical ranges associated to v_0 and $v_{\rm esc}$ [20–22]:

$$v_0=(220\pm 50)\ \ {\rm km\,s^{-1}}\quad (90\%\ \ {\rm C.L.}), \tag{9}$$

$$v_{\rm esc}=(450\div 650)\ \ {\rm km\,s^{-1}}\quad (90\%\ \ {\rm C.L.}). \tag{10}$$

The statistical method for the extraction of the annual-modulation region is the same as the one employed in Refs. [1–3], with a lower bound $m_\chi\geqslant 25$ GeV.

On the basis of the analytical properties of the time-modulated part of the detection rate [17], one expects that a variation in v_0 induces a sizeable modification in the range of m_χ, without affecting $\rho_\chi\sigma_{\rm scalar}^{\rm (nucleon)}$ significantly. Indeed, an increase (decrease) in v_0 is expected to extend the original DAMA-NaI region toward lower (larger) WIMP masses for kinematical reasons; $\rho_\chi\sigma_{\rm scalar}^{\rm (nucleon)}$ cannot appreciably change, since it acts as a normalization factor which is determined by

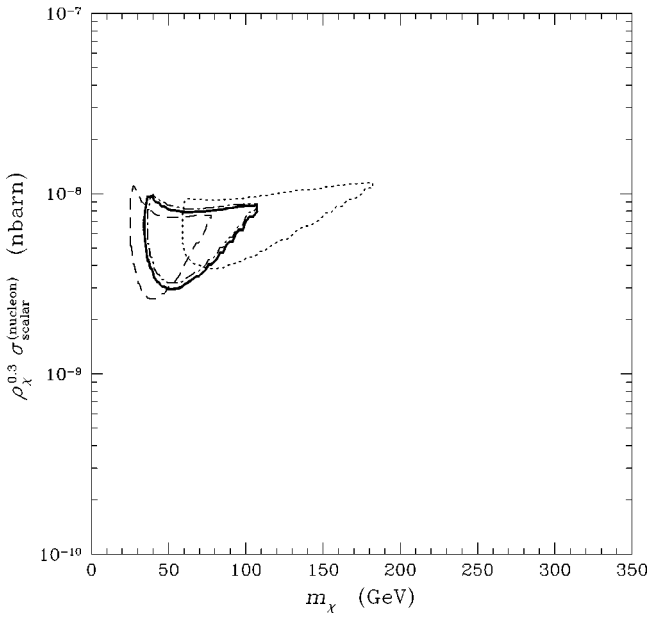

FIG. 1. Annual-modulation regions singled out by the DAMA-NaI experiment [3] in the plane $\rho_\chi^{0.3}\sigma_{\rm scalar}^{\rm (nucleon)} - m_\chi$ for various values of velocities v_0 and $v_{\rm esc}$: $v_0 = 220$ km s^{-1}, $v_{\rm esc} = 650$ km s^{-1} (solid line); $v_0 = 220$ km s^{-1}, $v_{\rm esc} = 450$ km s^{-1} (dot–dashed line); $v_0 = 170$ km s^{-1}, $v_{\rm esc} = 550$ km s^{-1} (dotted line); $v_0 = 270$ km s^{-1}, $v_{\rm esc} = 550$ km s^{-1} (dashed line). The contour line for $v_0 = 220$ km s^{-1}, $v_{\rm esc} = 550$ km s^{-1} is indistinguishable on the plot from the solid line. The quantity $\rho_\chi^{0.3}$ is the local neutralino matter density in units of 0.3 GeV cm^{-3}.

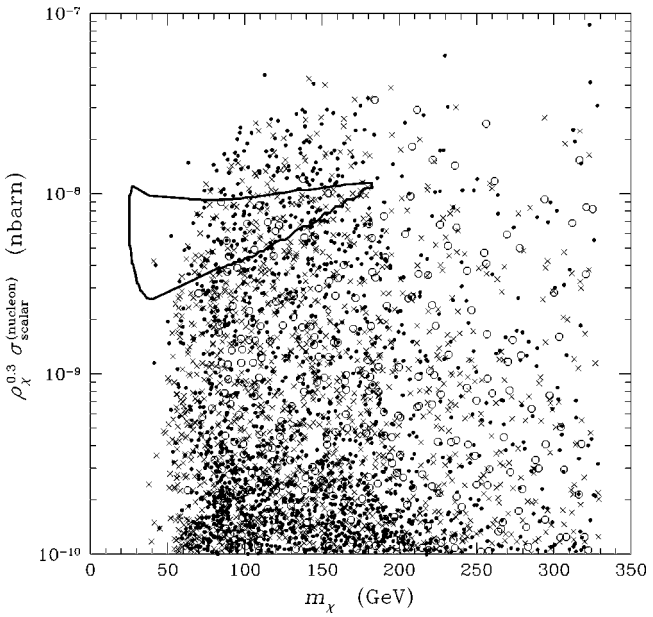

FIG. 2. The contour line delimits the annual-modulation region obtained by varying the velocities v_0 and $v_{\rm esc}$ over the ranges given in Eqs. (9)–(10). The scatter plot represents the theoretical predictions of a generic MSSM, as described in Sec. III. Different symbols identify different neutralino compositions: circles stand for a Higgsino, crosses for a gaugino, and dots for a mixed neutralino.

the size of the average detection rate. Also, no sizeable variation of both m_χ and $\rho_\chi \sigma_{\rm scalar}^{\rm (nucleon)}$ is expected from a variation in $v_{\rm esc}$, since the escape velocity provides a cutoff in the integral of Eq. (1) applying only on the flat tail of the velocity distribution $f(v)$.

We report in Fig. 1 the ($2-\sigma$ C.L.) annual-modulation regions extracted from the DAMA-NaI data of Ref. [3] (total exposure of 19 511 kg$\times$day) for sets of values for v_0 and $v_{\rm esc}$, which bracket the ranges given in Eqs. (9), (10). The $1-\sigma$ ranges for the relevant quantities are given in Table I. Notice that in Fig. 1 the density ρ_χ is given in units of 0.3 GeV cm^{-3}, i.e., $\rho_\chi^{0.3} \equiv \rho_\chi/(0.3 \text{ GeV cm}^{-3})$.

From the features displayed in Fig. 1 we notice that, as anticipated above: (i) the location of the annual-modulation region is rather sensitive to the velocity v_0, with a sizeable extension in the range of m_χ, but with small variations in $\rho_\chi \sigma_{\rm scalar}^{\rm (nucleon)}$; (ii) the annual-modulation region is essentially independent of $v_{\rm esc}$. From the results of Table I we conclude that the uncertainties in v_0 extend the range of m_χ, as singled out by the DAMA-NaI annual-modulation data, to (at $1-\sigma$ C.L.)

$$30 \text{ GeV} \lesssim m_\chi \lesssim 130 \text{ GeV}. \tag{11}$$

Taking into account the whole ranges of v_0 and $v_{\rm esc}$ [see Eqs. (9), (10)], we find the annual-modulation region which is depicted in Fig. 2. This region, which envelops the domains displayed in Fig. 1, will be hereafter referred to as region R_m.

It is worth noticing that this annual-modulation region might be further extended, if a possible bulk rotation of the dark matter halo is introduced. Unfortunately, halo models which take realistically into account this phenomenon are not yet available; however, effects of rotation of the dark matter halo on direct detection rates and ensuing upper bounds on cross sections have been addressed in some extreme models [23,24]. To obtain an estimate of the effects of a possible rotation of the isothermal sphere one can consider a class of models [25] which describe the fastest rotating steady state by means of the following recipe:

$$f_{\rm gal}^{+}(v^{\rm gal}) = \begin{cases} f_{\rm gal}(v^{\rm gal}), & v_\phi^{\rm gal} > 0, \\ 0, & v_\phi^{\rm gal} < 0, \end{cases} \tag{12}$$

TABLE I. Results of the maximum likelihood method when varying the velocity parameters (v_0 and $v_{\rm esc}$) of the WIMP velocity distribution. The values of m_χ and $\sigma_{\rm scalar}^{\rm (nucleon)}$ correspond to the minima of the maximum likelihood method (with 1σ error bars).

v_0 (km/s)	$v_{\rm esc}$ (km/s)	m_χ (GeV)	$\sigma_{\rm scalar}^{\rm (nucleon)}$ (10^{-9} nbarn)
220	450	59^{+17}_{-11}	$(7.3^{+0.5}_{-1.2})$
220	550	59^{+16}_{-13}	$(7.0^{+0.5}_{-1.2})$
220	650	59^{+17}_{-14}	$(7.0^{+0.4}_{-1.2})$
170	550	95^{+29}_{-20}	$(8.3^{+0.5}_{-1.2})$
270	550	41^{+14}_{-7}	$(6.8^{+0.4}_{-1.3})$

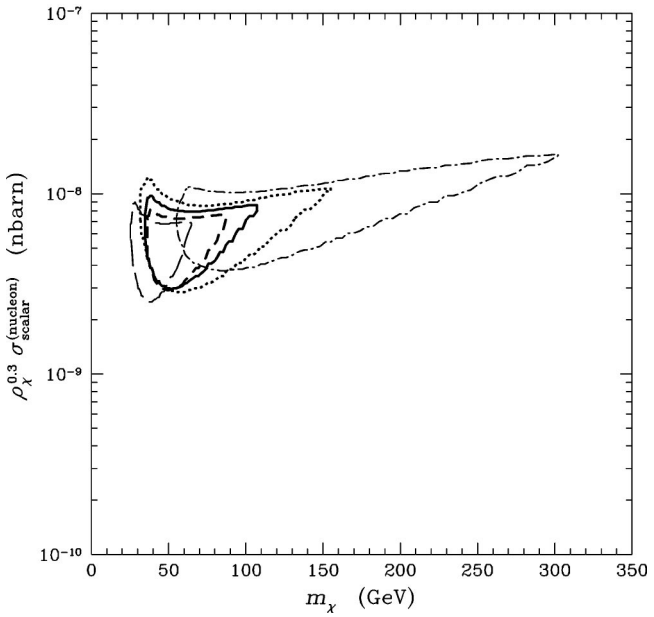

FIG. 3. Annual-modulation regions when a possible bulk rotation of the dark matter halo is taken into account. The contour lines refer to the following halo parameters: $v_0=220$ km s^{-1}, nonrotating halo (solid line); $v_0=220$ km s^{-1}, corotating halo with spin parameter $\lambda=0.05$ (dotted line); $v_0=220$ km s^{-1}, counter-rotating halo with $\lambda=0.05$ (dashed line); $v_0=170$ km s^{-1}, corotating halo with $\lambda=0.05$ (dot-dashed line); $v_0=270$ km s^{-1}, counter-rotating halo with $\lambda=0.05$ (long-dashed line). The escape velocity is fixed at the value $v_{\text{esc}}=550$ km s^{-1} for all the contours.

$$f_{\text{gal}}^{-}(v^{\text{gal}})=\begin{cases}0, & v_\phi^{\text{gal}}>0,\\ f_{\text{gal}}(v^{\text{gal}}), & v_\phi^{\text{gal}}<0,\end{cases} \tag{13}$$

where v_ϕ^{gal} is the azimuthal component of $\vec{v}^{\text{gal}}$.

Then one can combine the above functions in order to deal with a more general family of distribution functions $f_{\text{gal}}^{\text{rot}}(v^{\text{gal}})$, defined as [23]

$$f_{\text{gal}}^{\text{rot}}(v^{\text{gal}})=a f_{\text{gal}}^{+}(v^{\text{gal}})+(1-a) f_{\text{gal}}^{-}(v^{\text{gal}}), \tag{14}$$

where a is related to the dimensionless galactic angular momentum parameter λ by the relation $\lambda=0.36|a-0.5|$. In order to be consistent with the available extensive numerical work on galaxy formation, λ should not exceed the value 0.05 [26].

Adopting the expression in Eq. (14) for the velocity distribution function, one finds that the annual-modulation region may be extended to the domain depicted in Fig. 3, and the relevant range of m_χ would become (at $1-\sigma$ C.L.)

$$30\ \text{GeV}\leqslant m_\chi\leqslant 180\ \text{GeV}. \tag{15}$$

Although the possible occurrence of a bulk rotation of the dark matter halo is a quite interesting possibility deserving further investigation, all subsequent analyses of the present paper will refer to the region R_m, given in Fig. 2.

III. SUPERSYMMETRIC MODEL

The WIMP candidate considered in this paper is the neutralino, defined as the lowest-mass linear superposition of photino ($\tilde{\gamma}$), zino ($\tilde{Z}$) and the two Higgsino states ($\tilde{H}_1^0$, $\tilde{H}_2^0$) [27]

$$\chi\equiv a_1\tilde{\gamma}+a_2\tilde{Z}+a_3\tilde{H}_1^0+a_4\tilde{H}_2^0. \tag{16}$$

To classify the nature of the neutralino it is useful to define a parameter $P\equiv a_1^2+a_2^2$; hereafter the neutralino is called a gaugino, when $P>0.9$, is called mixed when $0.1\leqslant P\leqslant 0.9$, and a Higgsino when $P<0.1$.

The theoretical framework adopted here is the minimal supersymmetric extension of the standard model (MSSM) [27], which conveniently describes the supersymmetric phenomenology at the electroweak scale, without being constrained by too strong theoretical assumptions. Specific details of the scheme employed in this paper are given in Ref. [6]; here we only recall a few essentials.

The large number of free parameters inherent in the model is reduced to six independent ones, by imposing a few assumptions at the electroweak scale: (i) all trilinear parameters are set to zero except those of the third family, which are unified to a common value A; (ii) all squarks and sleptons soft-mass parameters are taken as degenerate: $m_{\tilde{l}_i}=m_{\tilde{q}_i}\equiv m_0$, (iii) the gaugino masses are assumed to unify at M_{GUT}, and this implies that the $U(1)$ and $SU(2)$ gaugino masses are related at the electroweak scale by $M_1=(5/3)\tan^2\theta_W M_2$.

The six independent parameters are taken to be $M_2,\mu,\tan\beta,m_A,m_0,A$, where μ is the Higgs-mixing parameter, $\tan\beta$ is the ratio of the two Higgs vacuum expectation values, and m_A is the mass of the neutral pseudoscalar Higgs boson. To get the scatter plots shown in this paper, the supersymmetric space has been randomly scanned with the parameters delimited by the following ranges: 10 GeV $\leqslant M_2\leqslant$ 1000 GeV, 10 GeV$\leqslant|\mu|\leqslant$1000 GeV, 80 GeV $\leqslant m_A\leqslant$1 TeV, 100 GeV$\leqslant m_0\leqslant$1 TeV, $-3\leqslant$A$\leqslant+3$, $1\leqslant\tan\beta\leqslant 50$. The scan has been performed linearly over M_2, μ, m_0, and A, and logarithmically over $\tan\beta$ and m_A.

Our supersymmetric parameter space is further constrained by all the experimental limits obtained from accelerators on supersymmetric and Higgs boson searches. The latest data from the CERN e^+e^- collider LEP2 on Higgs boson, neutralino, chargino, and sfermion masses are used [28]. Also the constraints due to the $b\rightarrow s+\gamma$ process [29,30] have been taken into account (see Ref. [6] for the theoretical details). The supersymmetric parameter space has also been constrained by the requirement that the neutralino is the lightest supersymmetric particle (LSP), i.e., regions where the gluino or squarks or sleptons are lighter than the neutralino have been excluded.

One further constraint is due to the requirement that the neutralino relic abundance does not exceed the cosmological bound, derivable from measurements of the age of the Universe [31] and of the Hubble constant [32]. We have adopted here a conservative upper bound, $\Omega_\chi h^2\leqslant 0.7$ [h is the usual

Hubble parameter, defined in terms of the present-day value H_0 of the Hubble constant as $h \equiv H_0/(100\ \mathrm{km\,s^{-1}\,Mpc^{-1}})$].

The neutralino relic abundance is calculated here as in Ref. [33]. Inclusion of coannihilation effects [34] in the calculation of $\Omega_\chi h^2$ turns out not to be necessary in the present analysis, since the instances under which these effects might be sizeable [34] are marginal for the supersymmetric configurations concerning the DAMA-NaI data.

Whenever we have to evaluate the neutralino local density without use of the DAMA data, we employ the rescaling procedure. This rescaling consists in assuming that the neutralino local density ρ_χ may be taken as $\rho_\chi = \xi \rho_l$ (ρ_l is the total local density of non-baryonic dark matter), with $\xi = \min\ [1, \Omega_\chi h^2/(\Omega h^2)_{\min}]$, i.e., ρ_χ may be set equal to ρ_l only when $\Omega_\chi h^2$ is larger than a minimal value $(\Omega h^2)_{\min}$, compatible with observational data and with large-scale structure calculations; otherwise, when $\Omega_\chi h^2$ turns out to be less than $(\Omega h^2)_{\min}$, and then the neutralino may only provide a fractional contribution $\Omega_\chi h^2/(\Omega h^2)_{\min}$ to Ωh^2, ρ_χ is reduced by the same fraction $\xi = \Omega_\chi h^2/(\Omega h^2)_{\min}$ as compared to ρ_l. The value to be assigned to $(\Omega h^2)_{\min}$ is somewhat arbitrary, in the range $0.01 \lesssim (\Omega h^2)_{\min} \lesssim 0.2$. In the present paper, whenever we have to apply rescaling, we use the value $(\Omega h^2)_{\min} = 0.01$, which is conservatively derived from the estimate $\Omega_{\mathrm{galactic}} \sim 0.03$.

In Fig. 2 we display our results for $\rho_\chi^{0.3}\ \sigma_{\mathrm{scalar}}^{(\mathrm{nucleon})}$ in the form of the scatter plot which is derived by scanning the supersymmetric parameter space over the grid defined above. For the evaluation of $\sigma_{\mathrm{scalar}}^{(\mathrm{nucleon})}$ we use the expressions given in Ref. [6]. The scatter plot shown in Fig. 2 is a consequence of (1) the experimental limits on supersymmety searches coming from accelerators and from the limits imposed by the $b \to s + \gamma$ radiative decay and (2) the interval over which the scan of the superymmetric parameter space is performed. For instance, neutralino searches at LEP constrain the mass of neutralino to be above about 30 GeV, hence a lower limit on the points in Fig. 2 as far as m_χ is concerned. Accelerator searches on the Higgs bosons constrain the mass and couplings of the supersymmetric Higgs bosons: this has a consequence of determining the maximal values which can be reached by the quantity $\rho_\chi^{0.3}\sigma_{\mathrm{scalar}}^{(\mathrm{nucleon})}$.

We notice that a host of configurations fall inside the region R_m; thus, the annual-modulation region is compatible with supersymmetric configurations currently allowed by accelerator constraints.

IV. INTERPRETATION OF THE ANNUAL-MODULATION DATA IN TERMS OF RELIC NEUTRALINOS

Let us turn now to the implications of the DAMA-NaI experimental data, once these are interpreted in terms of relic neutralinos. The cosmological properties are examined first; other prominent features of the relevant supersymmetric configurations will be examined afterwards.

A. Neutralino cosmological properties

For the derivation of the relic neutralino properties as regards its local density ρ_χ as well as its contribution to the average relic abundance $\Omega_\chi h^2$ compatible with region R_m, we adopt the straightforward procedure, outlined in Ref. [5], which does not require any use of rescaling in the local neutralino density. The method is the following: (1) We evaluate $\sigma_{\mathrm{scalar}}^{(\mathrm{nucleon})}$ and $\Omega_\chi h^2$ by varying the supersymmetric parameters over the grid and with the constraints defined in the previous section; (2) for any value of $[\rho_\chi \sigma_{\mathrm{scalar}}^{(\mathrm{nucleon})}]_{\mathrm{expt}}$ compatible with the region R_m we calculate ρ_χ as given by $\rho_\chi = [\rho_\chi \sigma_{\mathrm{scalar}}^{(\mathrm{nucleon})}]_{\mathrm{expt}}/\sigma_{\mathrm{scalar}}^{(\mathrm{nucleon})}$ and restrict the values of m_χ to stay inside the region R_m displayed in Fig. 2; (3) the results are then displayed in a scatter plot in the plane ρ_χ vs $\Omega_\chi h^2$.

Examples of our results are given in Figs. 4(a)–4(c) for a few experimentally allowed values of $\rho_\chi \sigma_{\mathrm{scalar}}^{(\mathrm{nucleon})}$, which bracket the range implied by the region R_m of Fig. 2. Parts (a)–(c) of Fig. 4 refer to the values $[\rho_\chi^{0.3}\sigma_{\mathrm{scalar}}^{(\mathrm{nucleon})}]_{\mathrm{expt}} = 4 \times 10^{-9}$ nbarn, 6×10^{-9} nbarn and 8×10^{-9} nbarn, respectively.

The two horizontal lines delimit the physical range $0.1\ \mathrm{GeV\,cm^{-3}} \lesssim \rho_l \lesssim 0.7\ \mathrm{GeV\,cm^{-3}}$ for the total local density of nonbaryonic dark matter. This (rather generous) range has been established by taking into account a possible flattening of the dark matter halo [35,36] and a possibly sizeable baryonic contribution to the galactic dark matter [37]. The solid vertical lines delimit the cosmologically interesting range $0.01 \lesssim \Omega_\chi h^2 \lesssim 0.7$. The two vertical dashed lines delimit the range: $0.02 \lesssim \Omega_\chi h^2 \lesssim 0.2$, which represents the most appealing interval. Indeed, some recent observations and analyses [38] indicate $0.1 \lesssim \Omega_{\mathrm{matter}} \lesssim 0.4$ (however, some other analyses, such as the one of Ref. [39] disfavor values on the low side of the quoted range for Ω_{matter}.) Combining this range with the one for h $0.55 \lesssim h \lesssim 0.80$ [32], we obtain $0.02 \lesssim \Omega_{\mathrm{CDM}} h^2 \lesssim 0.2$. The lower value of the $\Omega_{\mathrm{CDM}} h^2$ range takes into account that cold dark matter might provide only $\sim$(80–90) % of Ω_{matter}, the remaining fraction of $\sim$(10–20) % being due to hot and baryonic dark matter (as typical of models of cosmological structure formation, see, e.g., Ref. [40]). Our estimates for $\Omega_{\mathrm{CDM}} h^2$ are taken in the spirit of not being too restrictive in establishing the lower value for $\Omega_\chi h^2$ of cosmological interest (in agreement with what usually done also by other authors; for a recent reference see, for instance, Ref. [41]). Values of $\Omega_{\mathrm{CDM}} h^2$ as low as 0.02 may be rather unlikely, although not ruled out.

The two slant dot-dashed lines delimit the band where linear rescaling procedure for the local density is usually applied. In Figs. 4(a)–4(c) the upper dot-dashed line would refer to a rescaling with $(\Omega h^2)_{\min} = 0.01$, the lower one to the value $(\Omega h^2)_{\min} = 0.2$. However, notice that *in the derivation of the scatter plot of Figs. 4(a)–4(c), no use of rescaling for ρ_χ is made.*

With the aid of this kind of plot we can classify the supersymmetric configurations belonging to region R_m into various categories. Configurations whose representative points fall above the maximum value $\rho_\chi = 0.7\ \mathrm{GeV\,cm^{-3}}$ have to be excluded (we remind that those providing an $\Omega_\chi h^2 > 0.7$ are already disregarded from the very beginning). Among the allowed configurations, those falling in the region inside both the horizontal and solid vertical lines (called *A* hereafter) are very appealing, since they would represent

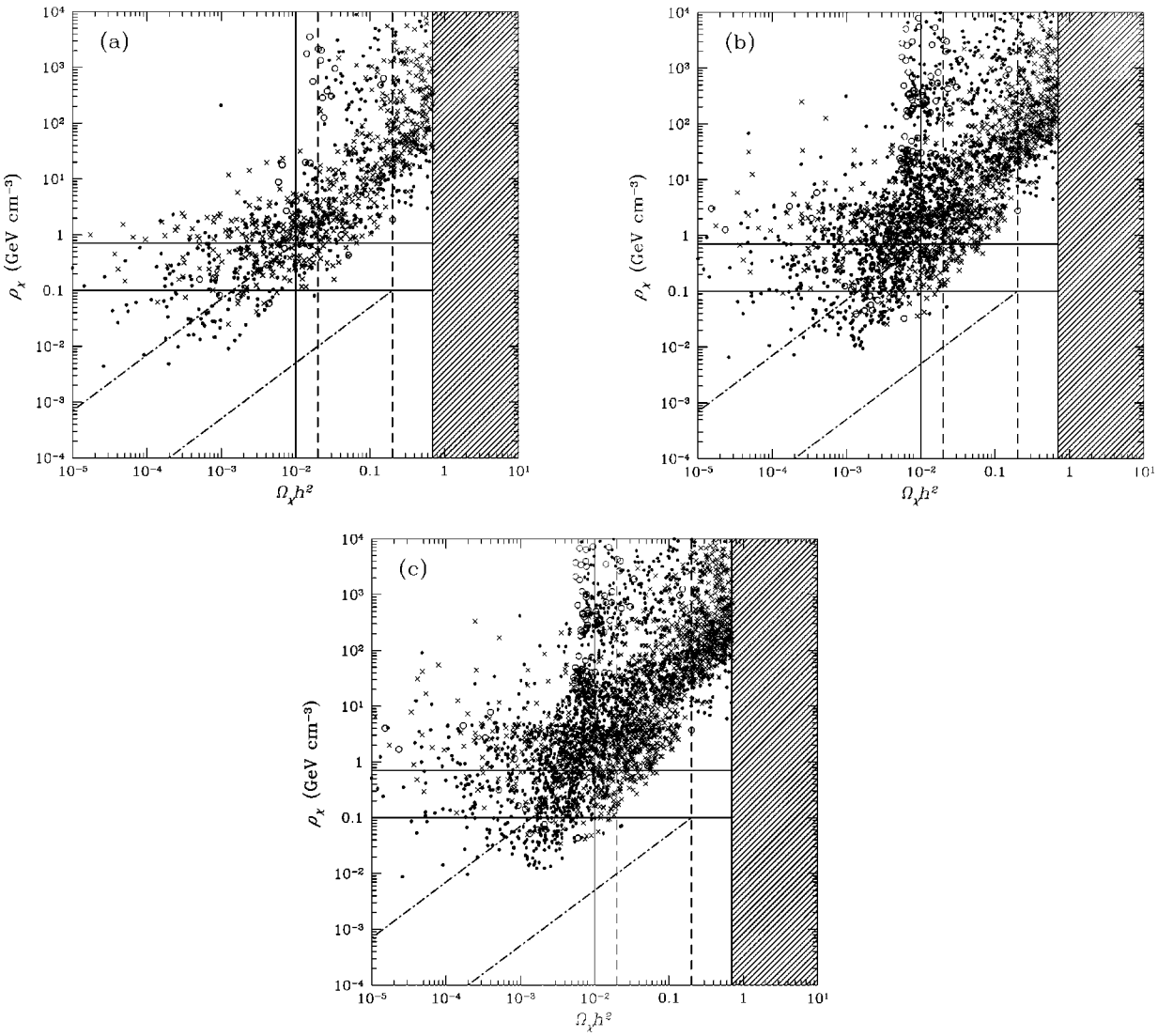

FIG. 4. The neutralino local density ρ_χ, calculated for fixed values of $[\rho_\chi^{0.3}\sigma_{\rm scalar}^{\rm nucleon}]_{\rm expt}$, is plotted versus the neutralino relic abundance $\Omega_\chi h^2$. For any value of $[\rho_\chi^{0.3}\sigma_{\rm scalar}^{\rm nucleon}]_{\rm expt}$ the neutralino mass is restricted to the range dictated by the contour line of Fig. 2. The different panels of the figure correspond to the following choices: (a) $[\rho_\chi^{0.3}\sigma_{\rm scalar}^{\rm nucleon}]_{\rm expt}=4\times10^{-9}$ nbarn and 28 GeV$\leqslant m_\chi \leqslant$88 GeV; (b) $[\rho_\chi^{0.3}\sigma_{\rm scalar}^{\rm nucleon}]_{\rm expt}=6\times10^{-9}$ nbarn and 25 GeV$\leqslant m_\chi \leqslant$131 GeV; (c) $[\rho_\chi^{0.3}\sigma_{\rm scalar}^{\rm nucleon}]_{\rm expt}=8\times10^{-9}$ nbarn and 25 GeV$\leqslant m_\chi \leqslant$156 GeV. The two horizontal lines delimit the physical range for the local density of nonbaryonic dark matter. The two solid vertical lines delimit the interval of $\Omega_\chi h^2$ of cosmological interest. The two vertical dashed lines delimit the preferred band for cold dark matter. The two slant dot-dashed lines delimit the band where linear rescaling procedure is usually applied. Different symbols identify different neutralino compositions: circles stand for a Higgsino, crosses for a gaugino and dots for a mixed neutralino.

situations where the neutralino could have the role of a dominant cold dark matter component; even more so, if the representative points fall in the subregion (called *B* hereafter) inside the vertical band delimited by dashed lines. Configurations which fall inside the band delimited by the slant dot-dashed lines denote situations where the neutralino can only provide a fraction of the cold dark matter both at the level of local density and at the level of the average Ω. Configurations above the upper dot-dashed line and below the upper horizontal solid line would imply a stronger clustering of neutralinos in our halo as compared to their average distribution in the Universe.

It is worth noticing a few important properties of the scatter plots shown in Figs. 4(a)–4(c).

(1) The scatter plots display a correlation between ρ_χ and $\Omega_\chi h^2$. This feature is expected on the basis of the following properties: (i) $\Omega_\chi h^2$ is roughly inversely proportional to the neutralino pair annihilation cross section, (ii) at fixed $[\rho_\chi \sigma_{\rm scalar}^{\rm (nucleon)}]_{\rm expt}$, ρ_χ is inversely proportional to $\sigma_{\rm scalar}^{\rm (nucleon)}$, (iii) the annihilation cross section and $\sigma_{\rm scalar}^{\rm (nucleon)}$ are usually correlated functions (i.e., they are both increasing or decreasing functions of the supersymmetric parameters, e.g., $\tan\beta$ or m_A).

(2) The domains covered by the supersymmetric configurations in regions *A* and *B* are slightly larger for smaller values of $[\rho_\chi \sigma_{\rm scalar}^{\rm (nucleon)}]_{\rm expt}$. This feature follows from the fact that $\sigma_{\rm scalar}^{\rm (nucleon)}$ is bounded from above by accelerator limits (mainly because of lower bounds on Higgs masses); this

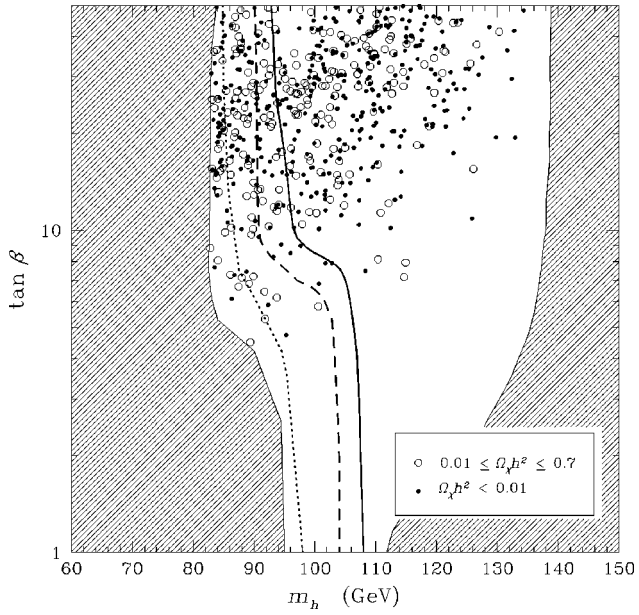

FIG. 5. Scatter plot for set S_m in the plane m_h–$\tan\beta$. The hatched region on the right is excluded by theory. The hatched region on the left is excluded by present LEP data at $\sqrt{s}=189$ GeV. The dotted and the dashed curves denote the reach of LEP2 at energies $\sqrt{s}=192$ GeV and $\sqrt{s}=200$ GeV, respectively. The solid line represents the 95% C.L. bound reachable at LEP2, in case of nondiscovery of a neutral Higgs boson.

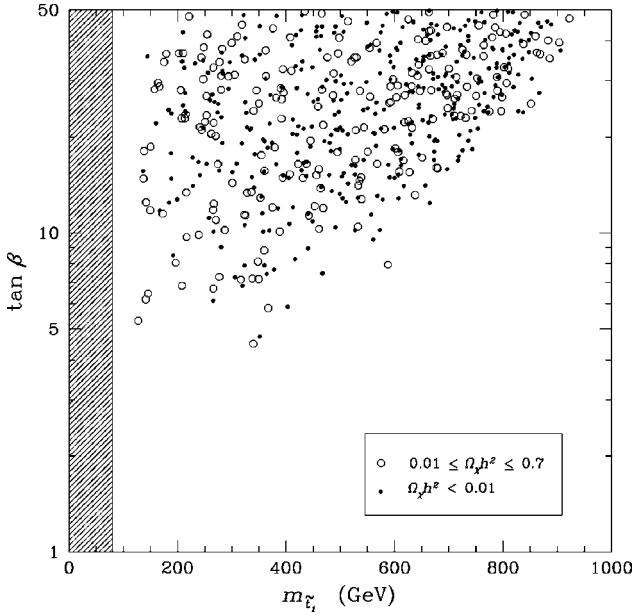

FIG. 6. Scatter plot for set S_m in the plane $m_{\tilde{t}_1}$–$\tan\beta$. The hatched region is excluded by LEP data.

implies for ρ_χ a lower bound, which, however, is less stringent at lower values of $[\rho_\chi \sigma^{(\text{nucleon})}_{\text{scalar}}]_{\text{expt}}$.

We can conclude that the DAMA-NaI data are compatible with a relic neutralino as a major component of dark matter in the universe.

B. Other properties of the supersymmetric configurations of set S_m

Apart from the cosmological properties previously discussed, one of the most interesting questions is whether the supersymmetric configurations, whose representative points fall inside the region R_m of Fig. 2 (hereafter denoted as configurations of set S_m), are explorable at accelerators of the present generation. This point was investigated in Ref. [6] in the case of the original DAMA-NaI annual-modulation region. Here we extend our considerations to the larger set S_m derived from region R_m.

The supersymmetric configurations of set S_m are constrained by the inequalities

$$\frac{[\rho_\chi \sigma^{(\text{nucleon})}_{\text{scalar}}]_{\text{expt}}}{\rho_{\chi,\max}} \leqslant \sigma^{(\text{nucleon})}_{\text{scalar}} \leqslant \frac{[\rho_\chi \sigma^{(\text{nucleon})}_{\text{scalar}}]_{\text{expt}}}{\rho_{\chi,\min}}, \quad (17)$$

where $\rho_{\chi,\min}=\xi\rho_{l,\min}=\xi\times 0.1$ GeV cm^{-3} and $\rho_{\chi,\max}=\xi\rho_{l,\max}=\xi\times 0.7$ GeV cm^{-3}, and $[\rho_\chi \sigma^{(\text{nucleon})}_{\text{scalar}}]_{\text{expt}}$ is any value inside region R_m as a function of m_χ.

Equation (17) implies interesting correlations among the supersymmetric parameters, as displayed in Figs. 5–7. The first of these figures shows the scatter plot of $\tan\beta$ versus the mass m_h of the lightest neutral CP-even Higgs boson (we recall that m_h may be derived from the supersymmetric parameters listed in Sec. III). The correlation displayed in Fig. 5 between $\tan\beta$ and m_h is implied by the fact that $\sigma^{(\text{nucleon})}_{\text{scalar}}$ is usually dominated by Higgs-exchange amplitudes, and these are in turn large for large values of $\tan\beta$ and small values of m_h. As is apparent in Fig. 5 a number of supersymmetric configurations of set S_m could still be explorable at LEP2, but the others require investigation at a high luminosity Fermilab Tevatron [42,43] or at the CERN Large

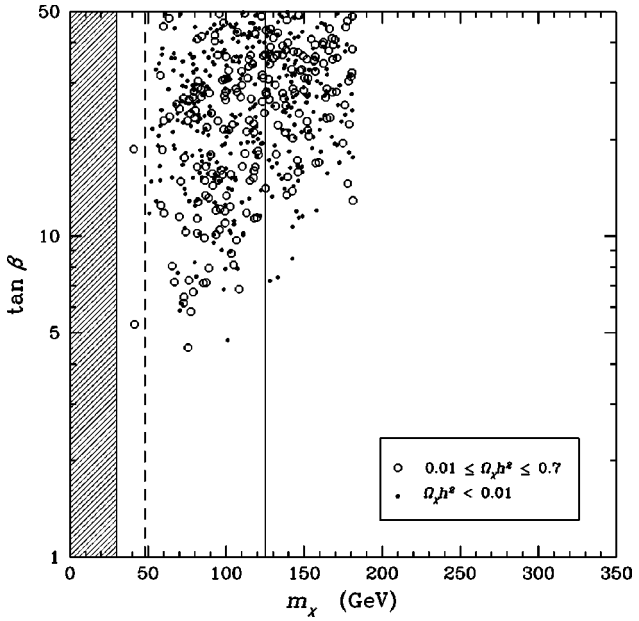

FIG. 7. Scatter plot for set S_m in the plane m_χ–$\tan\beta$. The hatched region on the left is excluded by present LEP data. The dashed and the solid vertical lines denote the reach of LEP2 and TeV33, respectively.

Hadron Collider LHC. Figure 6 shows a correlation between $\tan\beta$ and the mass of the lightest top-squark $m_{\tilde{t}_1}$. The reasons for this feature are more involved, and are discussed in Ref. [6].

A last plot, providing $\tan\beta$ versus m_χ, is given in Fig. 7. Again, a correlation shows up here for not too large values of $\tan\beta$. LEP2 can only provide an investigation up to $m_\chi \simeq 50$ GeV. The exploration up to ~ 125 GeV can be performed with Tevatron upgrades (under favorable conditions), while for higher values of m_χ LHC is needed.

V. CONCLUSIONS

We have investigated how the original DAMA-NaI annual-modulation region in the plane $\rho_\chi \sigma_{\rm scalar}^{\rm (nucleon)} - m_\chi$ is extended when the uncertainties in the galactic astrophysical velocities are taken into account. One of the most noticeable consequences is that the range for the neutralino mass becomes $30\ {\rm GeV} \lesssim m_\chi \lesssim 130\ {\rm GeV}$ at $1-\sigma$ C.L., with a further extension in the upper bound, when a possible bulk rotation of the dark matter halo is taken into account. However, the extension of the modulation region implies only slight modifications in the correlations among the supersymmetric parameters in the MSSM scheme.

We have found that a number of supersymmetric configurations singled out by the DAMA-NaI results have cosmological properties compatible with a relic neutralino as a dominant component of cold dark matter (on the average in our universe and in our galactic halo). It has also been discussed the discovery potential for the relevant supersymmetric configurations at accelerators of present generation.

Note added. During the completion of this work there appeared two preprints: hep-ph/9903467 (by L. Roszkowski) and hep-ph/9903468 (by M. Brhlik and L. Roszkowski), where considerations on the effect of the uncertainty in the velocity parameter v_0 on WIMP direct searches are presented. The extension of the original DAMA annual modulation region, due to this effect, qualitatively agrees with the one shown here in Fig. 1. In the preprints hep-ph/9903467 and hep-ph/9903468, at variance with the present paper, no dependence on $v_{\rm esc}$ and on a possible bulk dark matter rotation has been considered, neither the investigation on supersymmetric candidates has been carried out.

ACKNOWLEDGMENTS

A.B., F.D., and N.F. are grateful to Venya Berezinsky for interesting discussions about halo bulk rotations. This work was supported by DGICYT under Grant No. PB95-1077 and by the TMR network Grant No. ERBFMRXCT960090 of the European Union.

[1] R. Bernabei *et al.*, Phys. Lett. B **424**, 195 (1998).
[2] R. Bernabei *et al.*, Nuovo Cimento A **112**, 545 (1999).
[3] R. Bernabei *et al.*, Phys. Lett. B **450**, 448 (1999).
[4] A. Bottino, F. Donato, N. Fornengo, and S. Scopel, Phys. Lett. B **423**, 109 (1998).
[5] A. Bottino, F. Donato, N. Fornengo, and S. Scopel, hep-ph/9710295, Torino University Report No. DFTT 61/97.
[6] A. Bottino, F. Donato, N. Fornengo, and S. Scopel, Phys. Rev. D **59**, 095003 (1999).
[7] A. Bottino, F. Donato, N. Fornengo, and S. Scopel, Phys. Rev. D **59**, 095004 (1999).
[8] A. Bottino, F. Donato, N. Fornengo, and S. Scopel, Astropart. Phys. **10**, 203 (1999).
[9] For an analysis of the DAMA-NaI annual-modulation data in supergravity unified models, see also R. Arnowitt and P. Nath, Phys. Rev. D **60**, 044002 (1999).
[10] For preliminary results of our analysis see N. Fornengo, hep-ph/9812210, *Proceeding of the International Workshop on the Identification of Dark Matter (IDM98), Buxton, 1998*, edited by N. Spooner and V. Kudryavtsev (World Scientific, Singapore, 1999), p. 287; R. Bernabei and A. Bottino, talks given at the VIII International Workshop on Neutrino Telescopes (Venice, February 1999); transparencies available at http://axpd24.pd.infn.it/conference/venice99.html It is worth mentioning that the generic effect of astrophysical velocities uncertainties in particle dark matter direct search was already quantitatively addressed, for example, by Bacci *et al.*, Astropart. Phys. **2**, 117 (1994).
[11] A. Bottino, V. de Alfaro, N. Fornengo, G. Mignola, and S. Scopel, Astropart. Phys. **2**, 77 (1994).
[12] G. Jungman, M. Kamionkowski, and K. Griest, Phys. Rep. **267**, 195 (1996).
[13] R. Bernabei *et al.*, Phys. Lett. B **389**, 757 (1996).
[14] A. Bottino, F. Donato, G. Mignola, S. Scopel, P. Belli, and A. Incicchitti, Phys. Lett. B **402**, 113 (1997).
[15] R. H. Helm, Phys. Rev. **104**, 1466 (1956).
[16] J. Engel, Phys. Lett. B **264**, 114 (1991).
[17] K. Freese, J. Frieman, and A. Gould, Phys. Rev. D **37**, 3388 (1988).
[18] T. Damour and L. Krauss, Phys. Rev. D **59**, 063509 (1999).
[19] A. K. Drukier, K. Freese, and D. N. Spergel, Phys. Rev. D **33**, 3495 (1986).
[20] P. J. T. Leonard and S. Tremaine, Astrophys. J. **353**, 486 (1990).
[21] C. S. Kochanek, Astrophys. J. **457**, 228 (1996).
[22] K. M. Cudworth, Astron. J. **99**, 590 (1990).
[23] M. Kamionkowski and A. Kinkhabwala, Phys. Rev. D **57**, 3256 (1998).
[24] F. Donato, N. Fornengo, and S. Scopel, Astropart. Phys. **9**, 297 (1998).
[25] D. Lynden-Bell, Mon. Not. R. Astron. Soc. **120**, 204 (1960).
[26] S. Warren, P. J. Quinn, J. K. Salmon, and W. H. Zurek, Astrophys. J. **399**, 405 (1992); S. Cole and C. Lacey, Mon. Not. R. Astron. Soc. **281**, 716 (1996).
[27] H. P. Nilles, Phys. Rep. **110**, 1 (1984); H. E. Haber and G. L. Kane, *ibid.* **117**, 75 (1985). R. Barbieri, Riv. Nuovo Cimento **11**, 1 (1988).
[28] DELPHI Collaboration, V. Ruhlmann-Kleider, presentation at

the LEPC Conference, November 1998; R. Clare (L3 Collaboration), *ibid*.

[29] CLEO Collaboration, S. Glenn Report No. CLEO CONF 98-17, 1998, Proceedings of the International Conference on High Energy Physics, Vancouver, 1998, paper 1011.

[30] ALEPH Collaboration, R. Barate *et al.*, CERN Report No. CERN-EP/98-044, 1998.

[31] B. Chaboyer, P. Demarque, P. Kernan, and L. M. Krauss, Astrophys. J. **494**, 96 (1998).

[32] A. Sandage *et al.*, Astrophys. J. Lett. **460**, L15 (1996); W. L. Freedman, astro-ph/9706072, *Proceedings of the 18th Texas Symposium on Relativistic Astrophysics*, edited by A. Olinto, J. Frieman, and D. Schramm (World Scientific, Singapore, in press), and references quoted therein.

[33] A. Bottino, V. de Alfaro, N. Fornengo, G. Mignola, and M. Pignone, Astropart. Phys. **2**, 67 (1994).

[34] P. Binétruy, G. Girardi, and P. Salati, Nucl. Phys. **B237**, 285 (1984); K. Griest and D. Seckel, Phys. Rev. D **43**, 3191 (1991); S. Mizuta and M. Yamaguchi, Phys. Lett. B **298**, 120 (1993); J. Edsjö and P. Gondolo, Phys. Rev. D **56**, 1879 (1997).

[35] E. Gates, G. Gyuk, and M. S. Turner, Phys. Rev. Lett. **74**, 3724 (1995); Phys. Rev. D **53**, 4138 (1996).

[36] E. Gates, G. Gyuk, and M. S. Turner, Astrophys. J. Lett. **449**, L123 (1995).

[37] E. Gates, G. Gyuk, and M. S. Turner, astro-ph/9704253, *Proceedings of the 18th Texas Symposium on Relativistic Astrophysics*, edited by A. Olinto, J. Frieman, and D. Schramm (World Scientific, Singapore, in press).

[38] W. L. Freedman, R. Kirshner, and C. Lineweaver, talks given at the International Conference of Cosmology and Particle Physics (CAPP98), CERN, June 1998, wwwth.cern.ch/capp98/programme.html; M. White, Astrophys. J. **506**, 495 (1998); N. A. Bahcall and X. Fan, astro-ph/9804082; C. Lineweaver, astro-ph/9805326.

[39] M. Turner, astro-ph/9904051.

[40] J. R. Primack and M. A. K. Gross, astro-ph/9810204, Proceedings of the Xth Rencontres de Blois, *The Birth of Galaxies*, Chateau de Blois, June 1998.

[41] L. Bergström, T. Damour, J. Edsjo, L. M. Krauss, and P. Ullio, J. High Energy Phys. **8**, 010 (1999).

[42] Report of the TeV–2000 Study Group, edited by D. Amidei and R. Brock, Fermilab Report No. FERMILAB-PUB-96/082, 1996.

[43] H. Baer, B. W. Harris, and X. Tata, Phys. Rev. D **59**, 015003 (1999).